Supplementary Information (SI) for ChemComm.
This journal is © The Royal Society of Chemistry 2026

Supporting Information

1. Experimental Section

1.1 Preparation of Electrolytes

Sodium hexafluorophosphate ($NaPF_6$) were purchased from DodoChem and dried for over 12 hours in an argon-filled glovebox (Braun, O_2 <0.01 ppm, H_2O <0.01 ppm) before use. Dimethoxyethane (G1) and triglyme (G3) were purchased from Aladdin and dried with 3 Å level molecular sieve for 6 hours. P-G1 was prepared by dissolving 0.5 M $NaPF_6$ in G1. P-G1G3 was prepared by dissolving 0.5 M $NaPF_6$ in G1: G3 (4:1 vol.%). The preparation procedures of electrolytes were conducted in the glove box to strictly control the impurity content.

1.2 Preparation of Anodes and Cathodes

Anode material hard carbon (HC) (Kuraray, 80 wt%), carbon black (Super P, Canrd, 10 wt%), and polyvinylidene fluoride (PVDF, Canrd, 10 wt%) were mixed in N-methylpyrrolidone (NMP, Macklin) to form a homogeneous anode slurry. The slurry was coated onto aluminum current collectors and vacuum-dried at 60 °C (total mass loading: 1.5~2.5 mg cm^{-2}) for 12 hours (Vacuum drying oven, Shenzhenkejing). Active cathode material $Na_3V_2(PO_4)_3$ (NVP) (MTI Co., Ltd, 80 wt%), carbon black (Super P, Canrd, 10 wt%), and polyvinylidene fluoride (PVDF, Canrd, 10 wt%) were mixed in N-methylpyrrolidone (NMP, Macklin) to form a homogeneous cathode slurry. The slurry was coated onto aluminum current collectors and vacuum-dried at 120 °C (total mass loading: 3~5 mg cm^{-2}) for 12 hours. All electrodes were cut into circular pieces with a diameter of 11 mm. Higher-voltage layered oxide cathodes $NaNi_{1/3}Fe_{1/3}Mn_{1/3}O_2$ (NFM) and $NaNi_{0.24}Fe_{0.24}Mn_{0.24}Li_{0.07}Mg_{0.07}Ti_{0.07}Sb_{0.07}O_2$ (high entropy oxides, HEO) were synthesized via a conventional solid-state reaction method.

1.3 Electrochemical Measurements

CR2032-type cells were used for electrochemical measurements and all the batteries were assembled in an argon-filled glove box. Each HC||Na half-cell consisted of HC anode, porous glass fibers (Whatman®, GF/D) containing 150 μL electrolyte, and Na metal foil as the reference electrode. Each Na||NVP half-cell consisted of NVP cathode, porous glass fibers (Whatman®, GF/D) containing 150 μL electrolyte, and Na metal foil as the reference electrode. All batteries assembly processes were carried out in the argon-filled glove box with H_2O < 0.01 ppm and O_2 < 0.01 ppm. The operation voltage range of HC||Na, Na||NVP, Na||NFM, and Na||HEO half-cells are, respectively, 0.0~2.0, 2.0~3.8, 2.0~4.0, and 2.0~4.2 V. Pouch cell was directly assembled using raw HC and NVP.

1.4 Characterizations

Raman spectroscopy of solvents and electrolytes was conducted by Japan Horiba®

LabRAM HR Evolution with a 532 nm excitation laser. Nuclear magnetic resonance spectroscopy (NMR) of solvents and electrolytes was performed by Japan JEOL-JNM-ECZL G 600MHz to demonstrate the interactions between electrolyte components. DSC (Differential Scanning Calorimeter) curves were characterized by US TA Q2000 and carried out under a nitrogen atmosphere at a constant heating rate over the specified temperature range.

The surface properties of as-obtained HC anodes were investigated by X-ray photoelectron spectroscopy (XPS) using a US Thermo Scientific K-Alpha instrument, with a high-resolution scan step size of 0.05 eV. The SEI was characterized by time-of-flight secondary ion mass spectrometry (TOF-SIMS, IONTOF TOF-SIMS 5, Germany) with a mass resolution exceeding 5,000. The mass spectrometer is equipped with a 30 kV Bi+ analysis beam capable of depth profiling and high-resolution imaging analysis in high-current mode or burst alignment mode. The sputtering and analysis areas are 400 × 400 μm² and 200 × 200 μm², respectively. Samples were assembled in a glove box and then sealed for transfer to ensure contamination-free conditions. High-resolution transmission electron microscopy (HRTEM) images were captured using a US Thermo Fisher Talos F200S instrument. Scanning Electron Microscopy (SEM) images were captured using a CN CIQTEK SEM5000X instrument.

The ionic conductivities of the electrolytes were measured using Leici DDSJ-308F conductivity meter in the temperature chamber (Shanghai Husheng) from 60 to −60 °C. Electrochemical impedance spectroscopy (EIS) was performed using an Autolab potentiostat/galvanostat system (model PGSTAT302N, Metrohm®, Switzerland). The frequency range of EIS was from 10^5 Hz to 10^{-2} Hz. Before EIS measurements, HC||Na cells were galvanostatic charged/discharged at 0.2 C for 20 cycles at various temperatures and then kept at corresponding temperatures for 2 h. The activation energies (E_a) were calculated based on the following equation, $\frac{T}{R} = Aexp(\frac{-E_a}{k_bT})$,where R is the calculated impedance, T is the absolute temperature, k_b is the Boltzmann constant, and A is the pre-exponential factor.

1.5 Computational Methods

Quantum chemical calculations were carried out to determine the frontier molecular orbital (HOMO/LUMO) energy levels and Na^+ binding affinities of the target compounds using density functional theory (DFT) at the B3LYP/6-311G (d, p) level. Geometric optimizations and vibrational frequency analyses were performed with the B3LYP/6-311G (d, p) basis set. The binding energy (E_{bind}) was calculated as $E_{bind} = E_{AB} - E_A - E_B$, where E_{AB} represents the Gibbs free energy of the AB, E_A represents the Gibbs free energy of A, and E_B represents the

Gibbs free energy of B. Molecular dynamics (MD) simulations were conducted using Gromacs 2023.2 to model the electrolyte systems. Inter- and intramolecular interactions were described using the OPLS-AA force field, with solvent parameters generated via the LigParGen server and incorporated through itp files. The simulation workflow consisted of: (1) 2 ns NPT equilibration at 500 K; (2) 3 ns annealing from 330 K to 298 K; (3) 5 ns NPT followed by 10 ns NVT equilibration; and (4) 5 ns production runs for radial distribution function (RDF) and mean squared displacement (MSD). Temperature and pressure were controlled using the Nosé-Hoover thermostat and Berendsen barostat, respectively, with a 1 fs integration timestep. Trajectory visualization and post-processing were performed using VMD.

Adsorption energy calculations were performed using the Vienna Ab Initio Simulation Package (VASP) based on DFT. The exchange-correlation interactions were treated with the Generalized Gradient Approximation (GGA) in the Perdew-Burke-Ernzerhof (PBE) formulation, while core-valence interactions were described using the Projector Augmented Wave (PAW) method. The adsorption energy was defined as $E_{ads} = E_{AB} - E_A - E_B$, where E_{AB}, E_A, and E_B represent the total energies of the adsorbed system, the isolated adsorbate, and the clean substrate, respectively. A plane-wave cutoff energy of 400 eV was employed, and the Brillouin zone was sampled using the Monkhorst-Pack method with K-points optimized between $1 \times 1 \times 1$ and $3 \times 3 \times 1$ to ensure convergence. The energy convergence criteria for electronic and ionic relaxations were set to 1.0×10^{-4} eV and 1.0×10^{-3} eV, respectively, with a maximum force threshold of 0.02 eV/A. A DMol3 package that also adopting GGA/PBE as formulation was applied in the calculation of entropy values, while the plane-wave cutoff was set to 517 eV as well.

2. Supplementary Figures and Tables

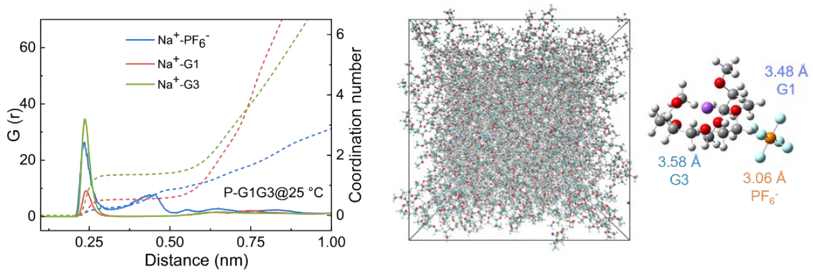

Figure S1. RDF of Na^+ solvation configurations in P-G1G3 at 25 °C and snapshot obtained from classical MD simulations of P-G1G3 at 25 °C.

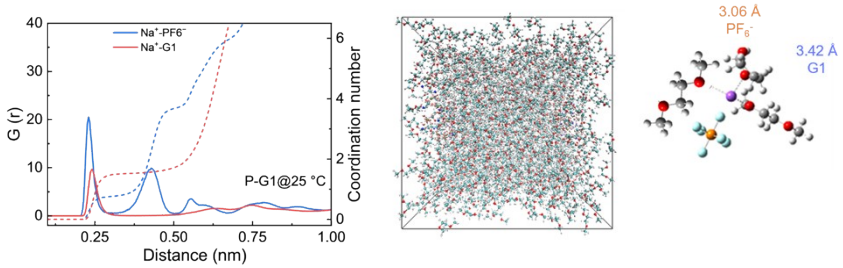

Figure S2. RDF of Na^+ solvation configurations in P-G1 at 25 °C and snapshot obtained from classical MD simulations of P-G1 at 25 °C.

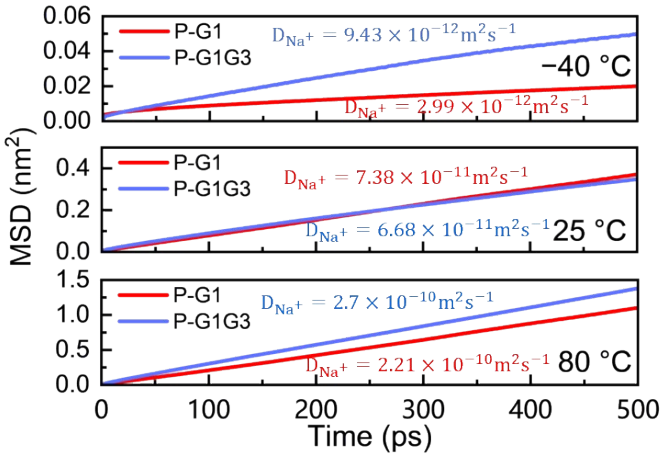

Figure S3. The mean squared displacement (MSD) of Na^+ in P-G1 and P-G1G3 at −40, 25, and 80 °C.

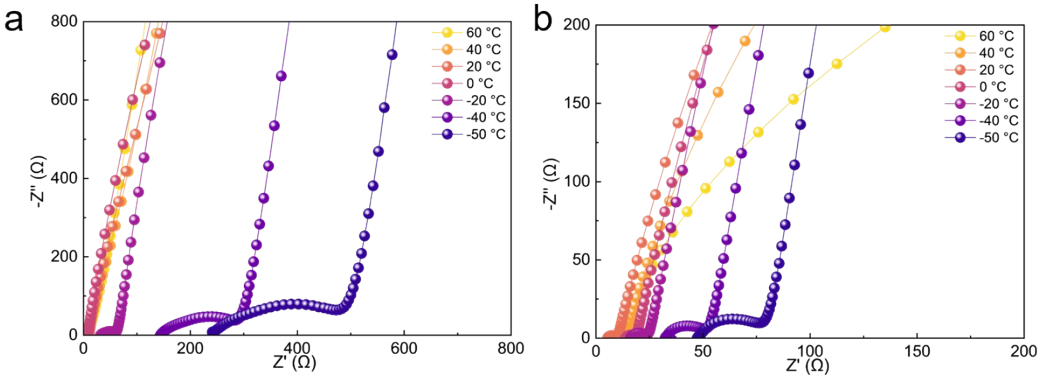

Figure S4. Nyquist plots of HC||Na half-cells with P-G1 (a) and P-G1G3 (b) from 60 °C to −50 °C.

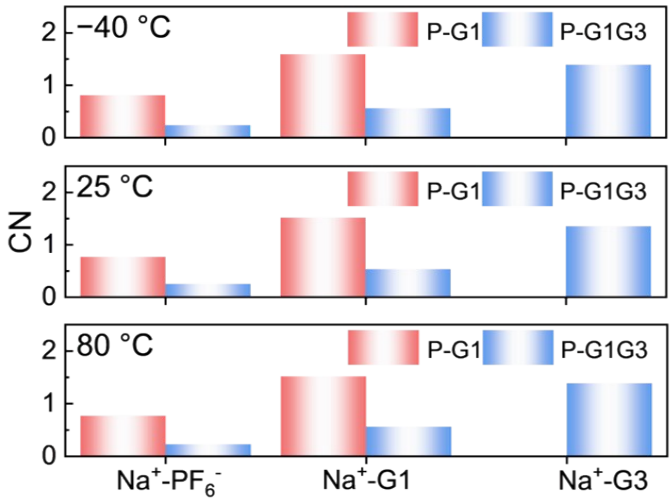

Figure S5. The coordination numbers (CNs) of different components in P-G1 and P-G1G3 at −40, 25, and 80 °C.

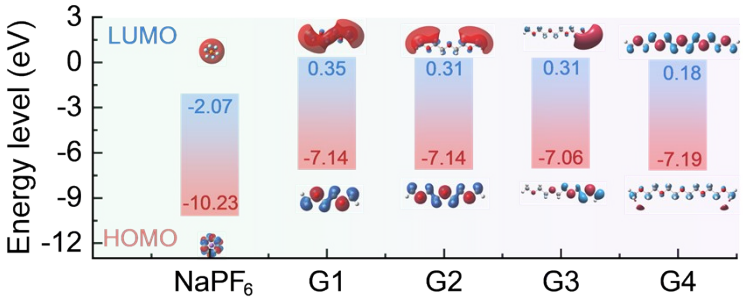

Figure S6. HOMO-LUMO energy levels of $NaPF_6$ and different ether molecules.

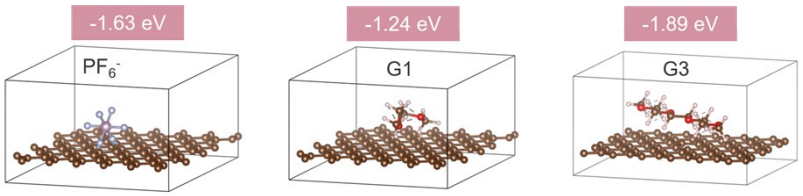

Figure S7. Adsorption energy of between the HC anode and different components in P-G1 and P-G1G3.

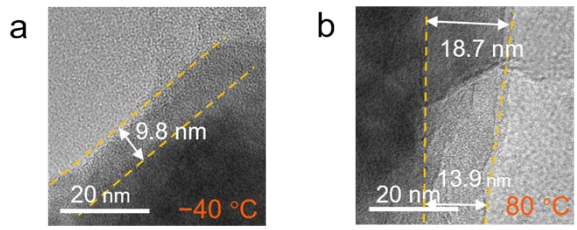

Figure S8. HRTEM images of cycled HC anodes in P-G1 at −40 °C (a) and 80 °C (b).

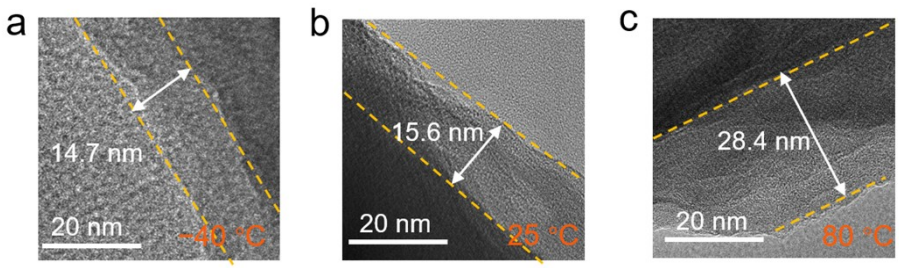

Figure S9. HRTEM images of cycled HC anodes in P-G1 at −40 °C (a), 25 °C (b), and 80 °C (c).

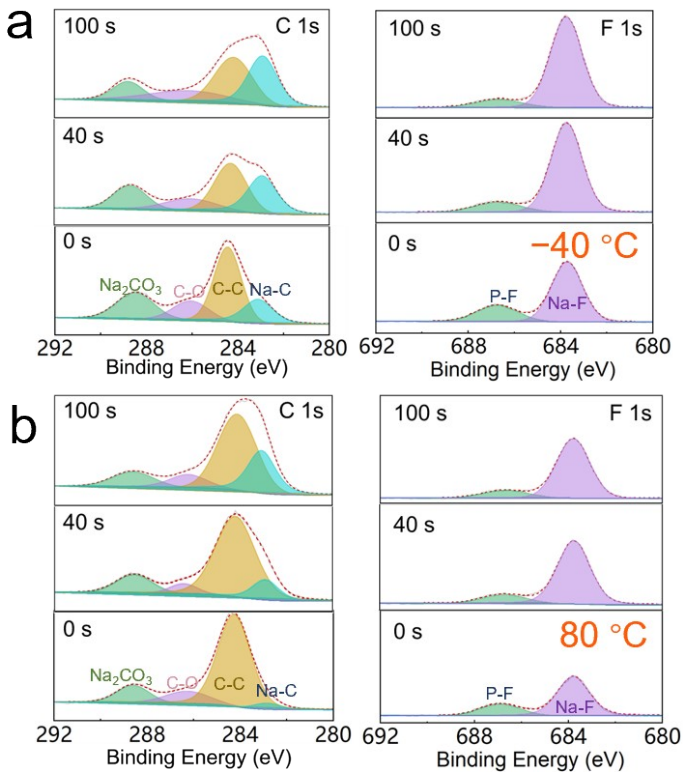

Figure S10. XPS C 1s and F 1s spectra of the cycled HC anodes after various sputtering times in P-G1G3 at −40 °C (a) and 80 °C (b).

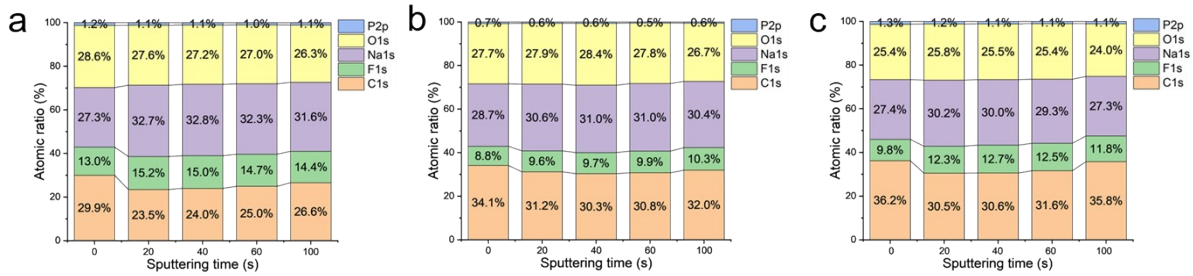

Figure S11. Atomic ratios of SEI components in P-G1G3 at −40 °C (a), 25 °C (b), and 80 °C (c).

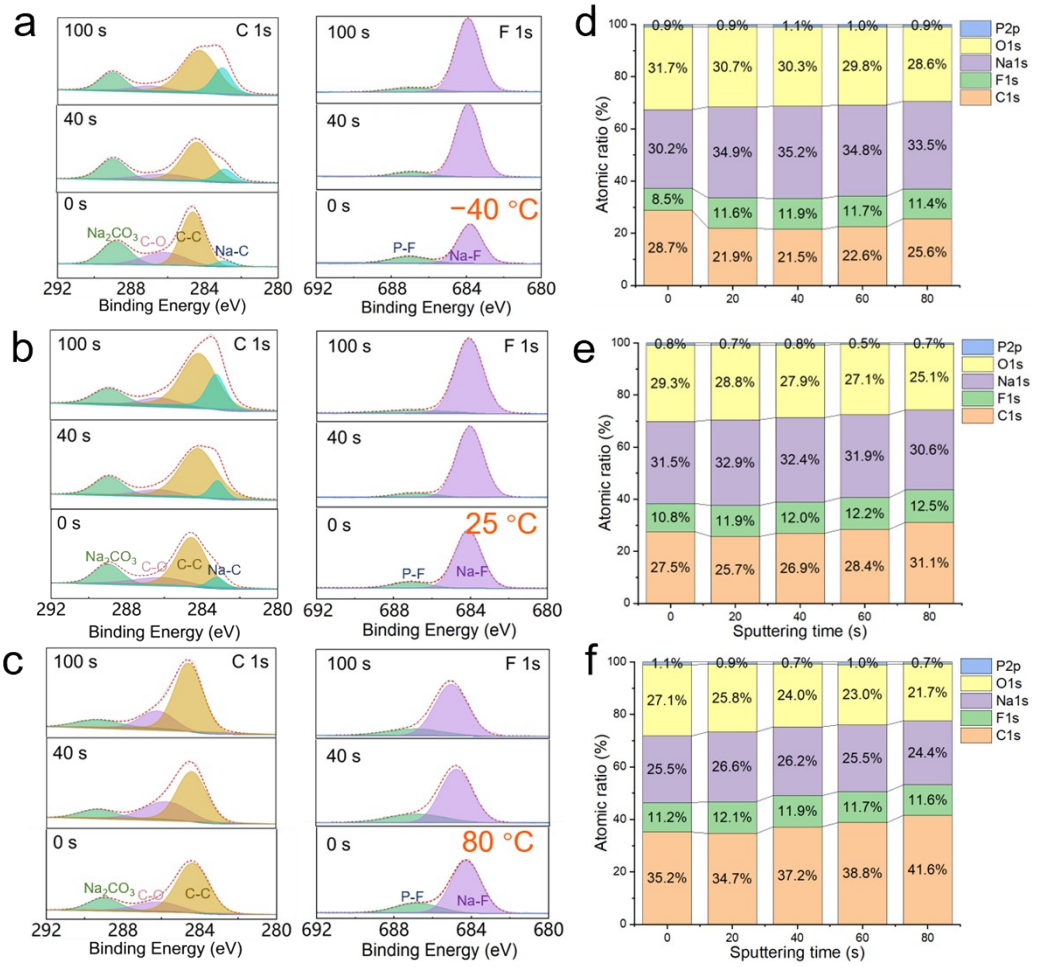

Figure S12. XPS C 1s and F 1s spectra of the cycled HC anodes after various sputtering times in P-G1 at −40 °C (a), 25 °C (b), and 80 °C (c). Atomic ratios of SEI components in P-G1 at −40 °C (d), 25 °C (e), and 80 °C (f).

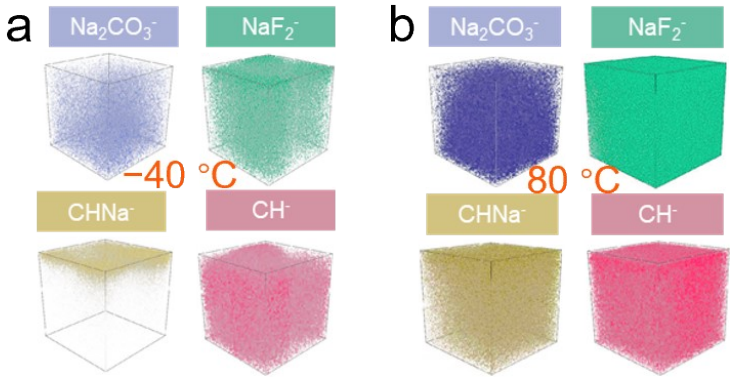

Figure S13. TOF-SIMS profiles of cycled HC anodes in P-G1G3 at −40 °C (a) and 80 °C (b).

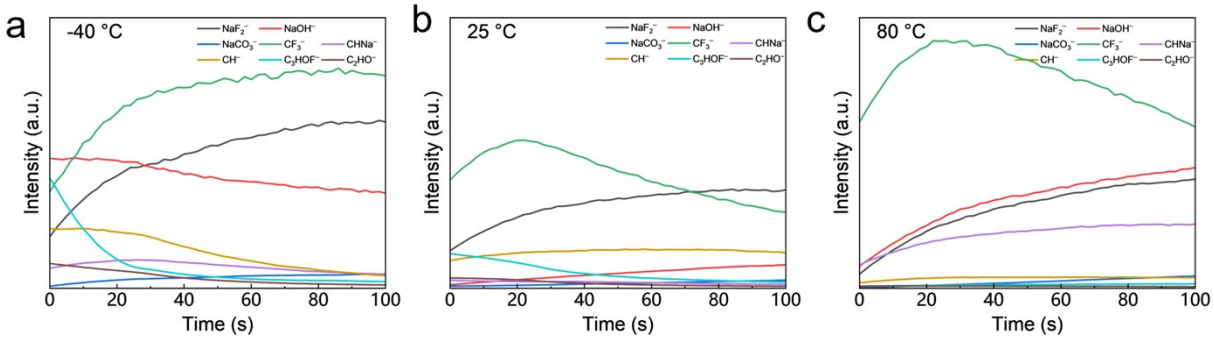

Figure S14. Depth profiles of TOF-SIMS tests for the SEIs of HC anodes formed P-G1G3 at −40 °C (a), 25 °C (b), and 80 °C (c).

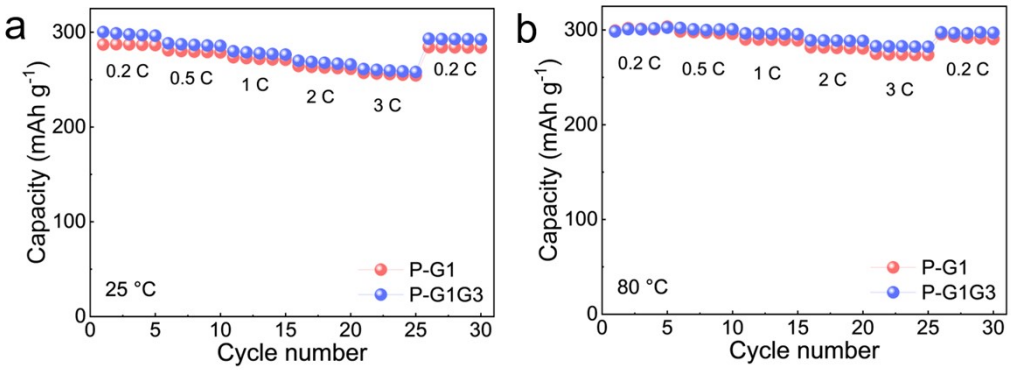

Figure S15. The rate performance of HC anodes in two electrolytes at 25 °C and 80 °C.

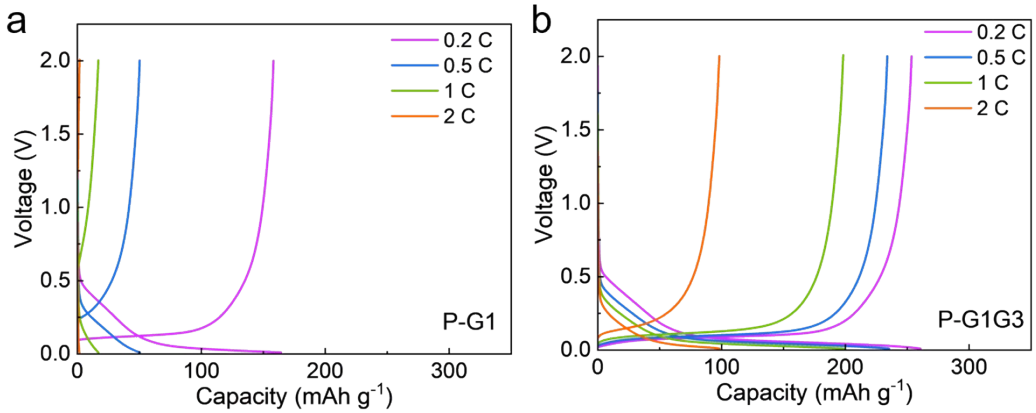

Figure S16. GCD voltage profiles of HC||Na half-cells with P-G1 and P-G1G3 (−40 °C) at different rates.

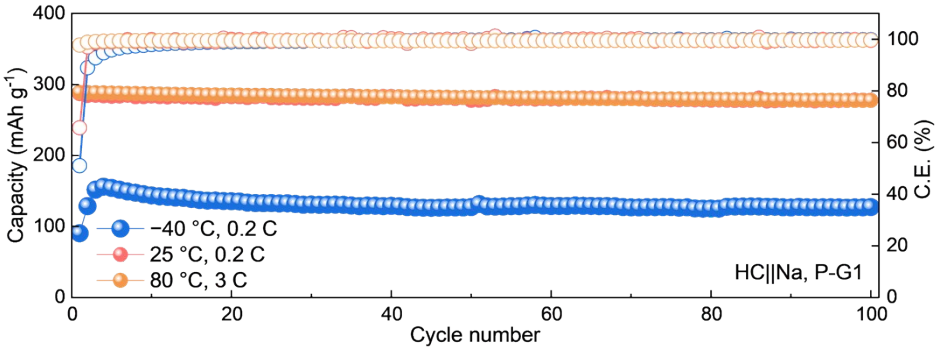

Figure S17. Cycling stability of HC||Na half-cells with P-G1 at different temperatures.

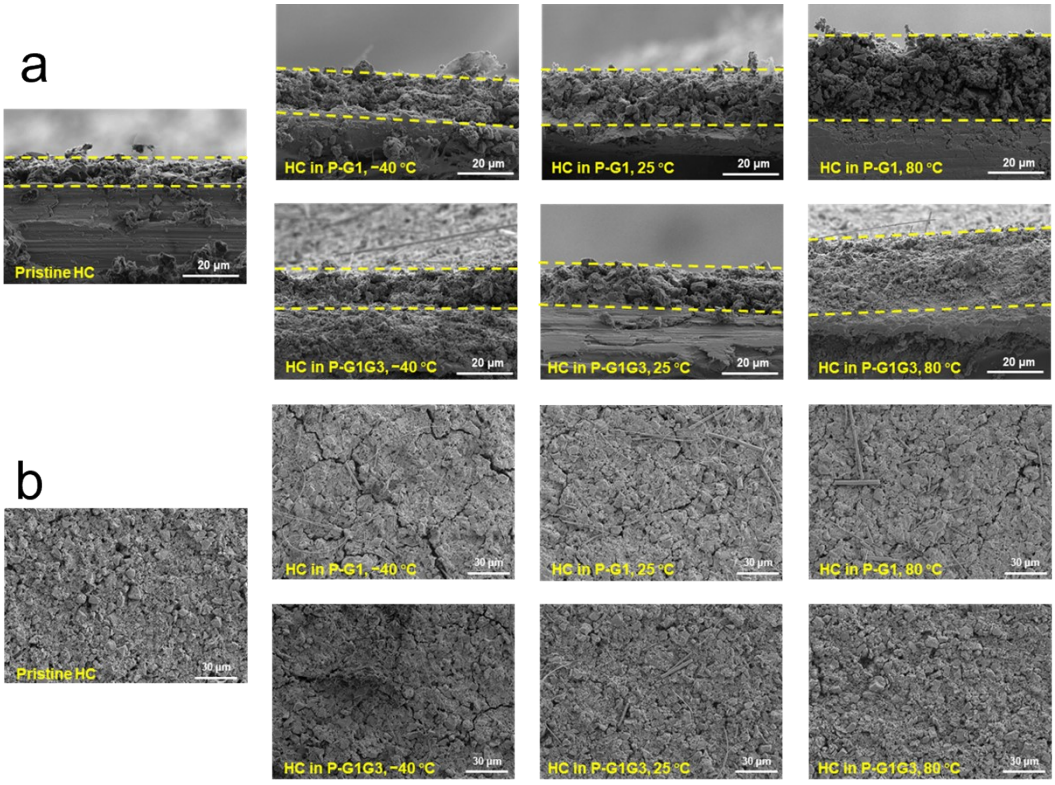

Figure S18. Cross-section SEM images (a) and surface SEM images (b) of pristine HC electrodes and cycled HC anodes from HC||Na cells in P-G1 and P-G1G3 after 100 cycles at different temperatures.

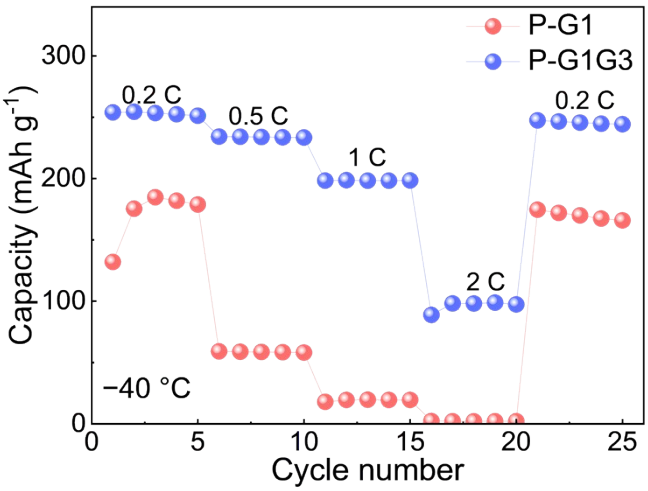

Figure S19. The rate performance of HC||Na half-cells in two electrolytes at –40 °C.

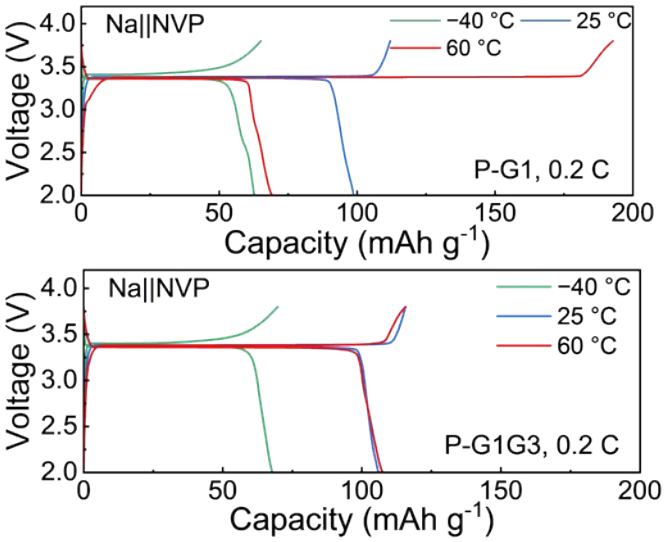

Figure S20. GCD voltage profiles of Na||NVP half-cells with two electrolytes (0.2 C) at −40, 25 and 60 °C.

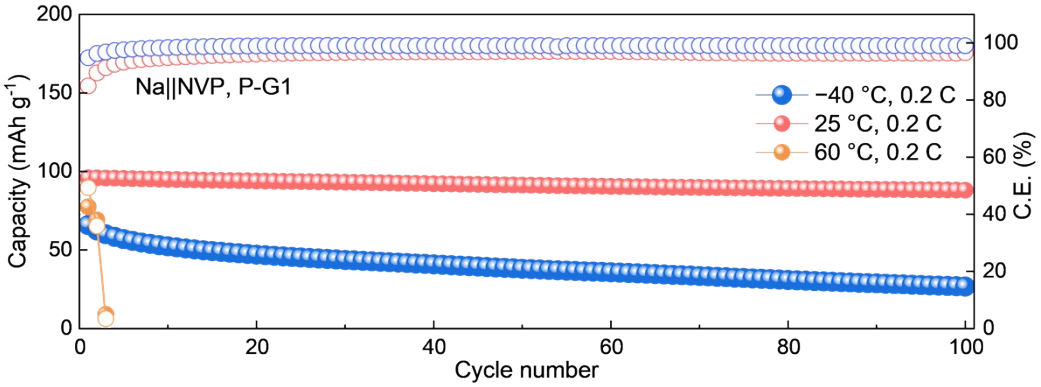

Figure S21. Cycling stability of Na||NVP half-cells with P-G1 at different temperatures.

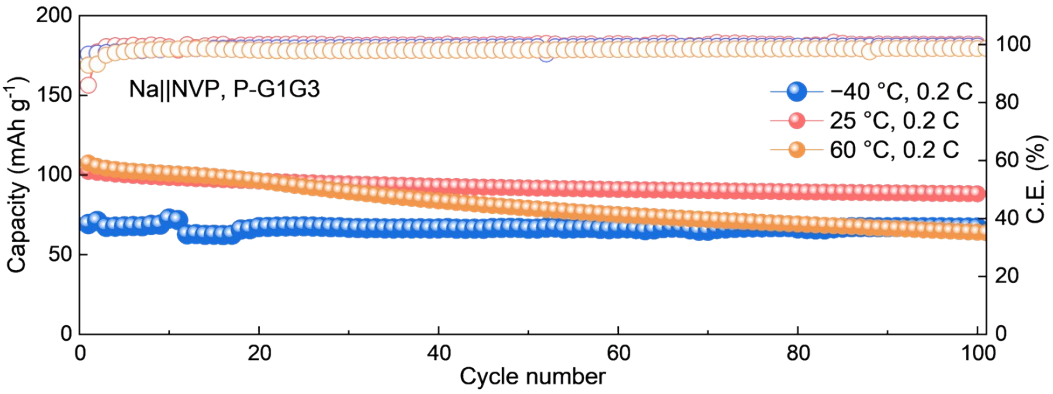

Figure S22. Cycling stability of Na||NVP half-cells with P-G1G3 at different temperatures.

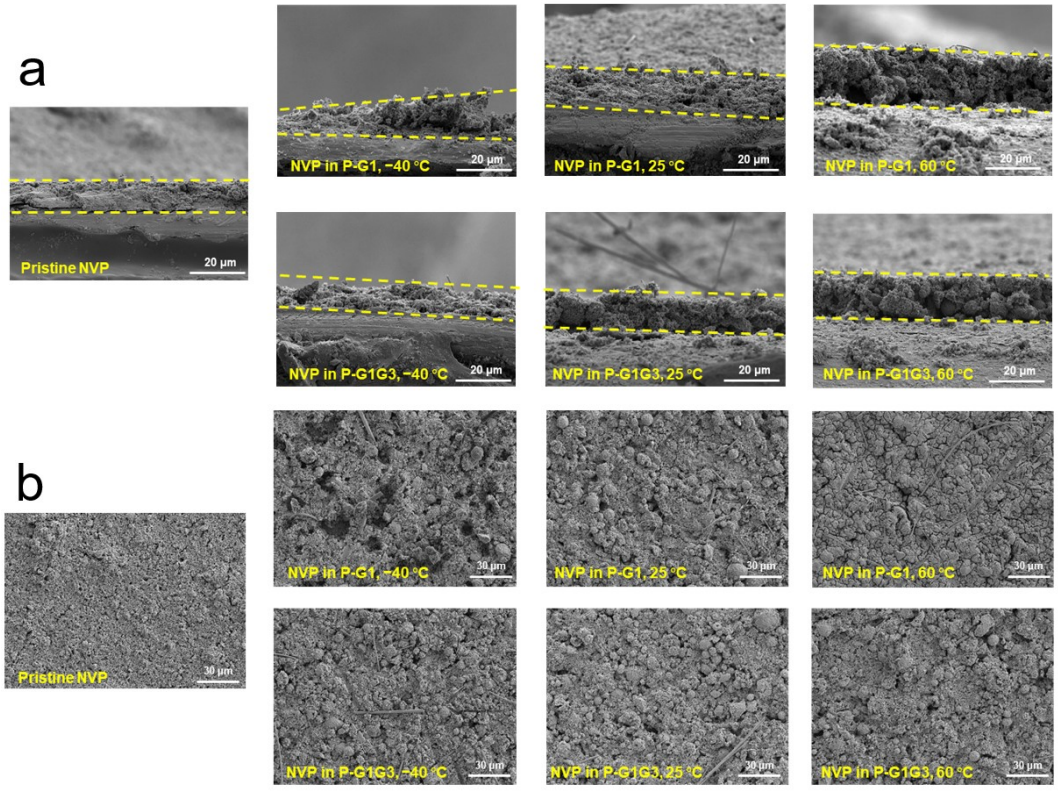

Figure S23. Cross-sectional SEM images (a) and surface SEM images (b) of pristine NVP electrodes and cycled NVP cathodes from Na||NVP cells in P-G1 and P-G1G3 after 100 cycles at different temperatures.

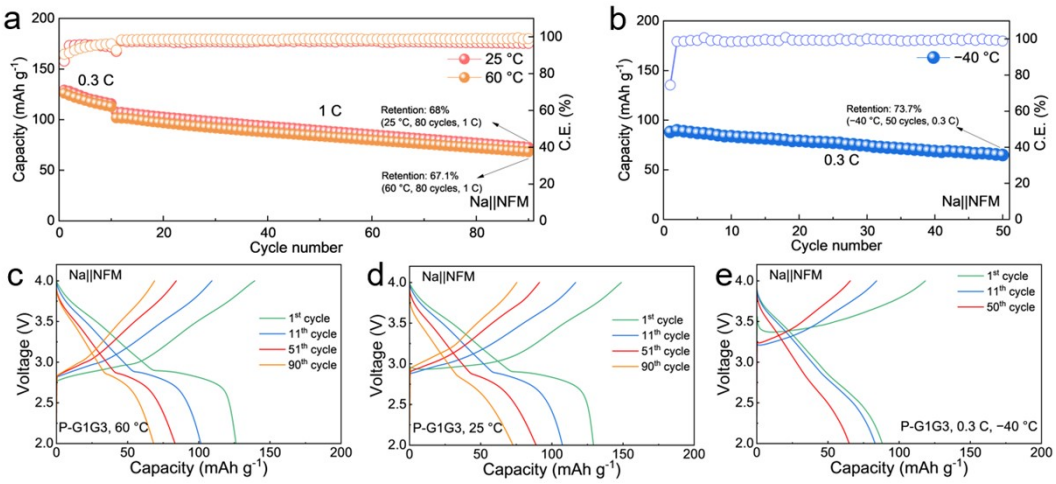

Figure S24. Cycling stability at 25 and 60 °C (a) and at −40 °C (b), together with corresponding GCD voltage profiles (c–e), of Na||NFM half-cells with P-G1G3 at different temperatures.

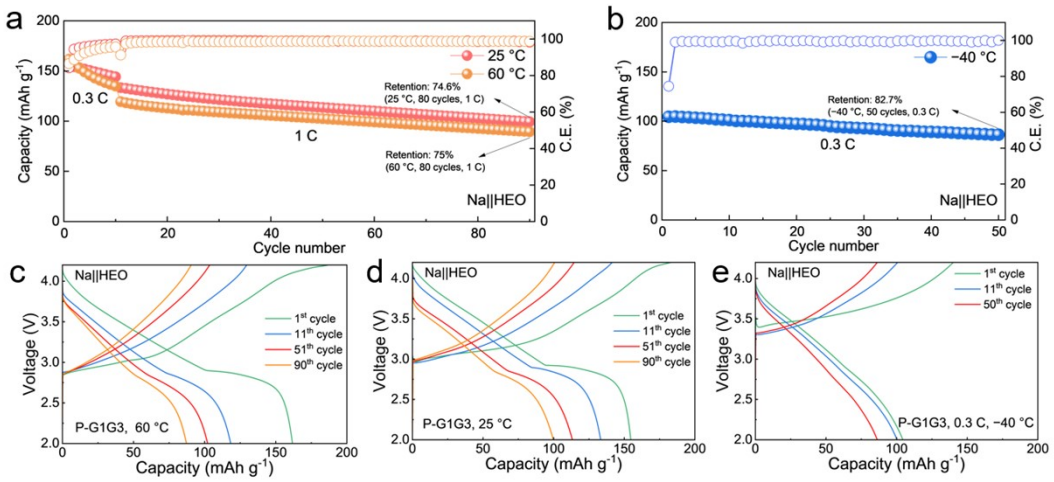

Figure S25. Cycling stability at 25 and 60 °C (a) and at −40 °C (b), together with corresponding GCD voltage profiles (c-e), of Na||HEO half-cells with P-G1G3 at different temperatures.

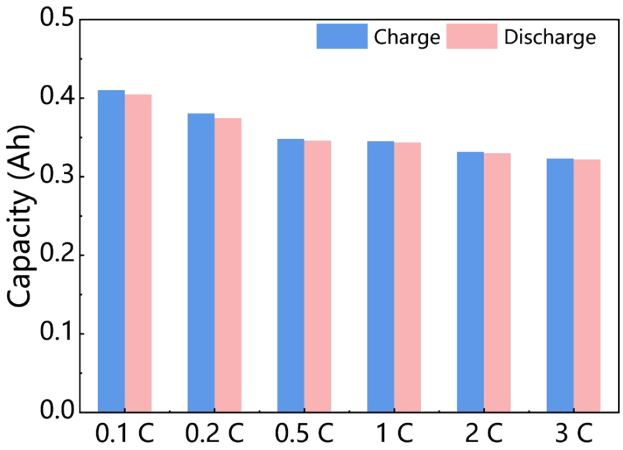

Figure S26. The rate performance of the HC||NVP pouch cell with P-G1G3 at different rates at 25 °C.

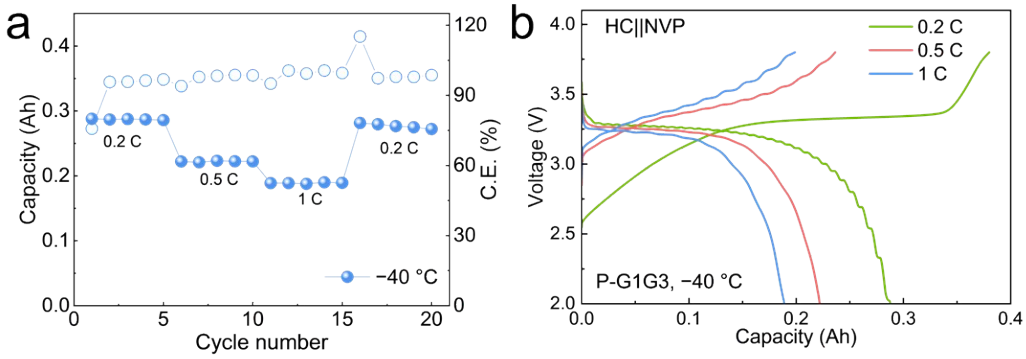

Figure S27. Low-temperature rate performance (a) and corresponding GCD voltage profiles (b) of the HC||NVP pouch cell using P-G1G3 at −40 °C.

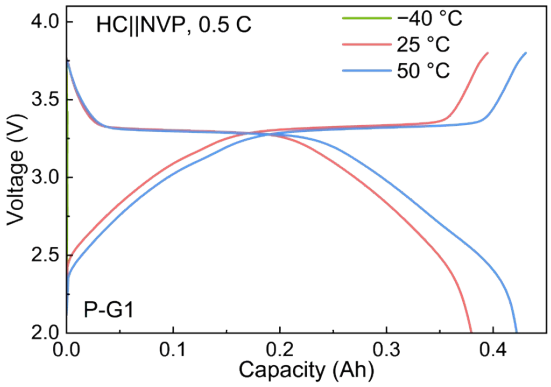

Figure S28. GCD voltage profiles of HC||NVP pouch cell with P-G1 (0.5 C) at −40, 25 and 50 °C.

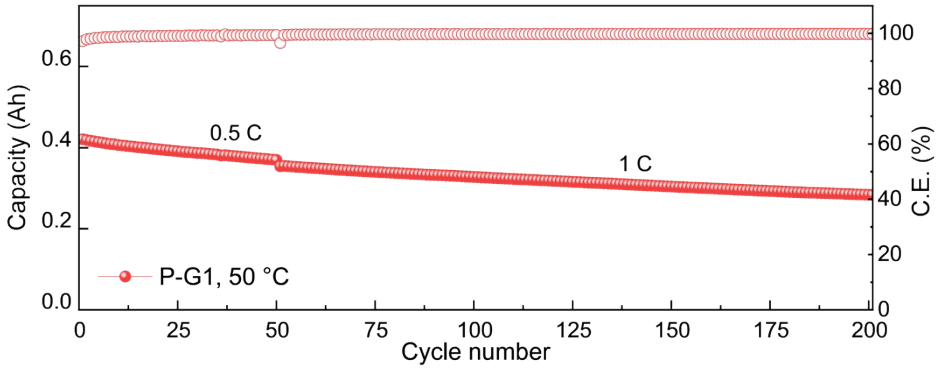

Figure S29. Cycling stability of HC||NVP pouch cell with P-G1 at 50 °C.

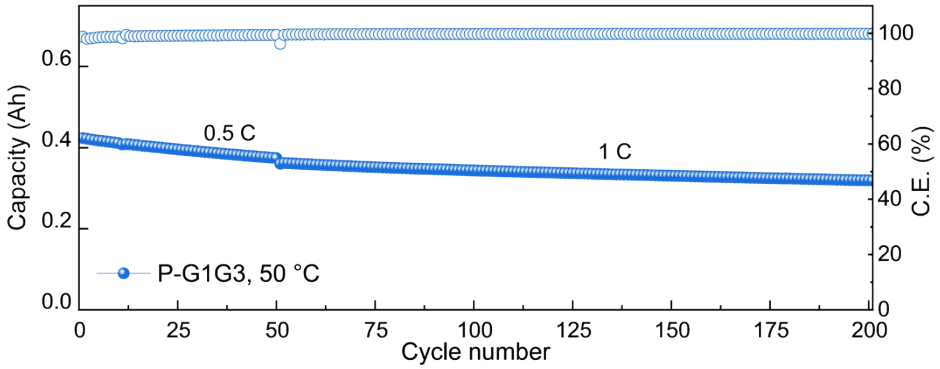

Figure S30. Cycling stability of HC||NVP pouch cell with P-G1G3 at 50 °C.

Table S1. Physicochemical properties of different solvents.

Solvent	Donor number	Dielectric constant	Freezing point (°C)	Boiling point (°C)
G1	20	7.2	–58	85
G2	19	7.2	–68	162
G3	14.0	7.6	–45	216
G4	16.6	7.9	–29.7	275

Table S2. The fitting results of EIS in HC||Na half-cells with P-G1 and P-G1G3 at different temperatures.

	60 °C	40 °C	20 °C	0 °C	–20 °C	–40 °C	–50 °C
R_{bulk} (P-G1)	5.63	5.49	5.77	7.54	30.83	141.9	236.3
R_{ct} (P-G1)	2.32	2.68	2.97	3.18	39.56	192.8	328.9
R_{bulk} (P-G1G3)	9.03	10.16	5.32	13.92	15.99	32.43	47.59
R_{ct} (P-G1G3)	2.69	3.31	4.68	4.58	8.59	21.22	35.04

Table S3. Comparison of electrochemical performance between this work and typical electrolytes in SIBs at wide temperatures.

Cell type	Electrolyte	Capacity at RT (mAh g^{-1})	Capacity at LT (mAh g^{-1})	Capacity at HT (mAh g^{-1})	Ref.
HC||Na	**0.5 M $NaPF_6$ in G1/G3**	**286.5 (60 mA g^{-1})**	**253.5 (60 mA g^{-1}, –40 °C)**	**302.5 (60 mA g^{-1}, 80 °C)**	**This work**
HC||Na	1.0 M $NaPF_6$ in G1/CPME	327.0 (100 mA g^{-1})	153.5 (50 mA g^{-1}, –20 °C)	\	1
HC||Na	1.0 M $NaPF_6$ in THF/Me-THF	270.3 (50 mA g^{-1})	243.2 (50 mA g^{-1}, –40 °C)	298 (50 mA g^{-1}, 55 °C)	2
HC||Na	0.8 M $NaPF_6$ in G2: MO	300.5 (20 mA g^{-1})	223.0 (20 mA g^{-1}, –40 °C)	\	3
HC||Na	1.0 M $NaPF_6$ in THF/Me-THF/AN	293.1 (100 mA g^{-1})	225.3 (100 mA g^{-1}, –40 °C)	301.4 (100 mA g^{-1}, 55 °C)	4
HC||Na	0.3 M $NaClO_4$ EC/PC with 5% FEC	219.8 (100 mA g^{-1})	150.2 (20 mA g^{-1}, –25 °C)	\	5
HC||Na	1.0 M $NaPF_6$ in PC/EMC/PFPN	251.0 (100 mA g^{-1})	179.0 (100 mA g^{-1}, 0 °C)	273.9 (100 mA g^{-1}, 60 °C)	6
HC||Na	1.0 M NaOTF in G2	327.0 (30 mA g^{-1})	189.0 (30 mA g^{-1}, –40 °C)	\	7

Abbreviations:

HT: high temperature RT: room temperature LT: low temperature.

CPME = cyclopentyl methyl ether THF = tetrahydrofuran MeTHF = 2-methyltetrahydrofuran

G2 = diglyme MO = 2-methyloxolane EC = ethylene carbonate

PC = propylene carbonate FEC = fluoroethylene carbonate EMC = ethyl methyl carbonate

$NaClO_4$ = sodium perchlorate NaOTF = sodium trifluoromethanesulfonate

Reference

1 Y. Zhou, W. Kong, H. Zhang, Y. Xue, Z. Huang and H. Xiang, *ACS Energy Lett.*, 2025, **10**, 2582–2592.

2 H. Fang, Y. Huang, W. Hu, Z. Song, X. Wei, J. Geng, Z. Jiang, H. Qu, J. Chen and F. Li, *Angew Chem Int Ed*, 2024, **63**, e202400539.

3 M. Li, Z. Liu, Y. Zhao, Z. Chen, Y. Zhang and N. Zhang, *Nat Commun*, 2026, **17**, 1478.

4 M. Wang, L. Yin, M. Zheng, X. Liu, C. Yang, W. Hu, J. Xie, R. Sun, J. Han, Y. You and J. Lu, *Nat Commun*, 2024, **15**, 8866.

5 L. Deng, K. Goh, F.-D. Yu, Y. Xia, Y.-S. Jiang, W. Ke, Y. Han, L.-F. Que, J. Zhou and Z.-B. Wang, *Energy Storage Materials*, 2022, **44**, 82–92.

6 E. Li, L. Liao, J. Huang, T. Lu, B. Dai, K. Zhang, X. Tang, S. Liu, L. Lei, D. Yin, J. Teng and J. Li, *Energy Storage Materials*, 2024, **73**, 103805.

7 B. Qiu, N. Sun, X. Li, R. A. Soomro, Y. Guan, H. Mi and B. Xu, *Advanced Functional Materials*, 2025, **35**, e12543.